Rev. Roum. Sci. Techn.– Électrotechn. et Énerg.
Vol. **17**, *3*, pp. 451–456, Bucarest, 2026

Automatique et ordinateurs
Automatic Control and Computer Sciences

PASSIVITY-BASED SLIDING MODE CONTROLLER/OBSERVER FOR A LIGHTWEIGHT ROBOTIC ARM

ADDA ADEL BELHERAZEM[1], MOHAMED DELLA KRACHAI [1], ZAKARIA BELLAHCENE[1]

Keywords: Lightweight robotic arm; Passivity-based control; Sliding mode observer; Euler-Lagrange formalism; Assumed modes approach.

This paper presents a passivity-based sliding-mode controller-observer for a two-link lightweight robotic arm that accounts for structural flexibility and payload mass. The system's dynamical model is obtained using the Euler-Lagrange formalism and the assumed modes method. The resulting mathematical model is highly nonlinear, with strong coupling between the rigid dynamics and the system's elastic behavior. To achieve accurate trajectory tracking with effective strain elimination, a full-order sliding-mode state observer is designed to estimate the state variables in the presence of parameter uncertainties and external perturbations. Then, the robust observer is combined with a passivity-based controller that uses the estimated states to achieve the desired trajectory, thereby improving system performance and robustness. The stability of the global system is demonstrated using Lyapunov theory and accounting for the passivity property, whereby the total energy is dissipated or stored within the system. The proposed controller/observer is evaluated using MATLAB/Simulink. Simulation results show good trajectory tracking with effective rejection of the external perturbations.

1. INTRODUCTION

Lightweight robotics arms have received a lot of attention during the last two decades due to their advantages compared to conventional robotic arms. Lightweight manipulators provide an adaptable solution that allows automation, accuracy, and increased productivity in numerous applications, including aerospace, healthcare, and the manufacturing industry. They can perform multiple tasks and even complex movements with high precision and low energy consumption. However, we also need to address the inherent challenges that come with the use of lightweight materials. The tip vibrations caused by distributed structural flexibility and robotic linkage result in a very complex dynamic model with distributed parameters. In addition, the inherent non-minimum phase behavior and the parametric variation (payload mass, structural damping coefficients, etc.) prevent the system from reaching the control objectives and complicate the control task. [1] In order to achieve an accurate trajectory tracking with an effective rejection of the external perturbations, several control strategies have been investigated for a multi-link lightweight manipulator in the literature. To achieve accurate trajectory tracking with effective rejection of external perturbations, a few control strategies have been investigated for a multi-link lightweight manipulator in the literature. In [2,16,17], the authors address the control of an uncertain rigid flexible manipulator using adaptive neural tracking and motion planning. To achieve position control, virtual damping and online path correction are used to determine the manipulator's motion. As demonstrated by the simulation results, the motion planning and tracking controllers outperform other control strategies, and the effectiveness of the recommended control strategy is also confirmed.

In [3], a composite learning sliding mode control of a two-link elastic manipulator is presented. The adaptive scheme is developed using a new neural network update law and a disturbance observer, and simulation results confirm the design concept that compound-learning can successfully complete the estimation task. In [4], a sliding mode controller is designed to control a flexible joint manipulator. The proposed controller ensures stabilization and demonstrates robust tracking performance, as verified through simulation results.

[5] presents an adaptive passive controller for a single-link flexible manipulator with a parametric variation. This controller includes the passivity-based approach and an adjustment mechanism that ensures online parameter estimation. Simulations illustrate the theoretical results and show that the controller implements asymptotic trajectory tracking and suppresses tip vibrations effectively.

Reference [6] proposes using a genetic algorithm to actively control the vibration of a flexible manipulator. A novel intelligent optimizer known as the genetic algorithm with parameter exchanger (GAPE) was used to adapt the PID controller. The performance of PID and common genetic algorithms was examined. The findings demonstrate that PID-GAPE offers superior results in vibration attenuation.

[7] developed a Luenberger observer that can estimate the state variables using one sensor that measures the velocity of the motor. The simulation results demonstrated that the five unmeasured signals (motor angle, gear angle, link angle, angular velocity of gear, and angular velocity of link) could all be accurately estimated by the suggested control algorithm with minimum errors.

This work builds upon our preliminary research on passivity-based control of flexible manipulators presented in [1,13,15], which relied on direct feedback via physical sensors; this dependency increases cost, complexity, and susceptibility to sensor noise.

The main contribution of this paper is to shift from a hardware-dependent paradigm to a software-based estimation framework by designing a full-order sliding mode observer. This robust observer can estimate all state variables based on the available system inputs and outputs despite the measurement uncertainties and the external perturbations. These estimates are then used in the design of the passivity-based controller, which ensures that the whole system remains passive, which guarantees stability and robustness. The combination of the robust state observer with the passivity-based control law ensures cost reduction by minimizing reliance on physical sensors and provides accurate state estimation and robustness against measurement noise and external disturbances. This paper's remaining sections are assembled as follows. The mathematical model of the two-link lightweight robotic arm based on the Euler-Lagrange formalism is presented in Section 2, and the passivity-based controller is presented in Section 3. Section 4 is dedicated to

[1] Faculty of Electrical Engineering, University of Sciences & Technologies of Oran BP1505 El M'Naouer 31000, Algeria.
E-mails: addaadel.belherazem@univ-usto.dz, mohamed.dellakrachai@univ-usto.dz, zakaria.bellahcene@univ-usto.dz

DOI: 10.59277/RRST-EE.2026.3.19

designing the sliding mode state observer. Simulation results are presented in Section 4. The conclusion is presented in Section 5.

2. PROBLEM FORMULATION

A two-link lightweight robotic arm is depicted in Fig. (1), the inertial coordinate frame is denoted X_0Y_0 , the i^{th} link rigid body coordinate frame is denoted X_iY_i, and the motion coordinate frame is $\widehat{X_i}\widehat{X_i}$. The i^{th} link length is L_i with uniform mass density ρ_i. The first motor clamps the first link at the rotor, and the second motor is clamped at the first link tip. E and I are defined as the two links' individual Young's modulus and area moment of inertia, respectively. The elastic deflection of the i^{th} link is $w_i(x_i, t)$, which is smaller than the link's length. The angular coordinates are θ_1,θ_2. An inertial payload mass Mp with moment of inertia J_p is connected at the tip of the second link [9]. The two links are considered as Euler-Bernoulli beams. We assume that the robotic arm only moves on the horizontal plane, unaffected by shear deformation.

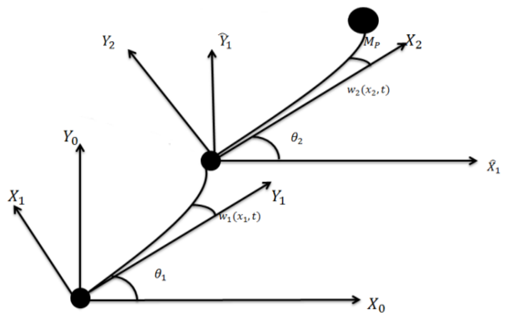

Fig.1 – A two-link lightweight robotic arm.

A finite-dimensional expression of each link deflection is formulated as

$$w_i(x_i, t) = \sum_{j=1}^{m_i} \phi_{ij}(x_i)q_{ij}(t), \tag{1}$$

where $\phi_{ij}(x_i)$ are the j^{th} modal displacement and the j^{th} flexible mode shape function for the i^{th} link, which satisfy the geometric boundary conditions given in (8). m_i is the number of the flexible modes adopted for the i^{th} link, in our case, two modes for each link are required $m_1 = m_2 = 2$.

The equation of motion of a two-link lightweight robotic arm is derived using the Euler-Lagrange formalism as follows [10]:

$$M(Q)\ddot{Q} + C(Q,\dot{Q})\dot{Q} + g(Q) = \tau_i, \tag{2}$$

where $Q = [\theta_1, \theta_2, q_{11}, q_{12}, q_{21}, q_{22}]^T = [\theta \;\; q]^T$ is the generalized coordinates vector; $M(Q) \in \Re^{n\mathrm{x}n}$ is the inertia matrix of the system; $C(Q,\dot{Q}),\dot{Q} \in \Re^n$ is the Coriolis and centripetal forces vector; g is the gravity vector; $\tau_i = [\tau_1\, \tau_2\; 0\; 0\; 0\; 0]^T = [\tau \;\; 0]^T$ refers to the actuator torques vector; Q $\dot{Q}$, $\ddot{Q}$ are n−dimensional vectors representing joint displacements, velocities, and accelerations, respectively.

Equation (2) can be written in the explicit compact form:

$$\begin{pmatrix} M_{11} & M_{12} & M_{13} & M_{14} & M_{15} & M_{16} \\ 0 & M_{22} & M_{23} & M_{24} & M_{25} & M_{26} \\ 0 & 0 & M_{33} & M_{34} & M_{35} & M_{36} \\ 0 & 0 & 0 & M_{44} & M_{45} & M_{46} \\ 0 & 0 & 0 & 0 & M_{55} & M_{56} \\ 0 & 0 & 0 & 0 & 0 & M_{66} \end{pmatrix} \begin{pmatrix} \ddot{\theta}_1 \\ \ddot{\theta}_2 \\ \ddot{q}_{11} \\ \ddot{q}_{12} \\ \ddot{q}_{21} \\ \ddot{q}_{22} \end{pmatrix} +$$

$$\begin{pmatrix} C_1(Q,\dot{Q})\dot{Q} \\ C_2(Q,\dot{Q})\dot{Q} \\ C_3(Q,\dot{Q})\dot{Q} \\ C_4(Q,\dot{Q})\dot{Q} \\ C_5(Q,\dot{Q})\dot{Q} \\ C_6(Q,\dot{Q})\dot{Q} \end{pmatrix} + \begin{pmatrix} g_1(Q) \\ g_2(Q) \\ g_3(Q) \\ g_4(Q) \\ g_5(Q) \\ g_6(Q) \end{pmatrix} = \begin{pmatrix} \tau_1 \\ \tau_2 \\ 0 \\ 0 \\ 0 \\ 0 \end{pmatrix}. \tag{3}$$

3. PASSIVITY BASED CONTROLLER DESIGN

Let's define the desired trajectory vector which includes the desired rigid and flexible coordinates: $Q_d = [\theta_d, q_d]^T$, and its successive derivatives $\dot{Q}_d = [\dot{\theta}_d, \dot{q}_d]$, $\ddot{Q}_d = [\ddot{\theta}_d, \ddot{q}_d]$.

The control aim is to optimize the manipulator's applied torque (2) so that the trajectory of the system Q follows nearly the intended trajectory Q_d. Let's define the displacement error vector e_q by

$$e_Q = Q - Q_d = \begin{pmatrix} e_r \\ e_f \end{pmatrix} = \begin{pmatrix} \theta - \theta_d \\ q - q_d \end{pmatrix} = \begin{pmatrix} \theta - \theta_d \\ q \end{pmatrix}, \tag{4}$$

where q_d is set to zero to suppress vibrations.

To eliminate steady-state position errors, we restrict them to lie on the following sliding surface

$$s = \dot{e}_Q + \Lambda e_Q = 0, \tag{5}$$

with an adjustable diagonal positive gain matrix Λ.

The storage function in s-coordinate is [11]:

$$H = \frac{1}{2}s^T M(Q)s. \tag{6}$$

Differentiating it yields

$$\dot{H} = s^T M(Q)\dot{s} + \frac{1}{2}s^T \dot{M}(Q)s, \tag{7}$$

$$\dot{H} = s^T\left(M\ddot{e}_Q + M\Lambda e_Q + \frac{1}{2}\dot{M}s\right), \tag{8}$$

$$\dot{H} = s^T\left(M\ddot{q} - M\ddot{q}_d + M\Lambda e_Q + \frac{1}{2}\dot{M}s\right). \tag{9}$$

Then, substituting $M\ddot{q}$ from the dynamic eq. (2)

$$M\ddot{q} = \tau_i - C\dot{Q} - g = \tau_i - C\left(s + \dot{Q}_d - \Lambda e_Q\right) - g, \tag{10}$$

yields

$$\dot{H} = s^T\left(\tau_i - C\dot{Q} - g - M\ddot{q}_d + M\Lambda e_Q + \frac{1}{2}\dot{M}s\right), \tag{11}$$

$$\dot{H} = s^T\begin{pmatrix} \tau_i - M\ddot{Q}_d + M\Lambda e_Q - C\dot{Q}_d + \\ C\Lambda e_Q - g + \frac{1}{2}\left(\dot{M}s - 2C\right)s \end{pmatrix}. \tag{12}$$

Using the skew-symmetry property, we obtain

$$\dot{H} = s^T\left(\tau_i - M\ddot{Q}_d + M\Lambda e_Q - C\dot{Q}_d + C\Lambda e_Q -\right)g. \tag{13}$$

Let's introduce a virtual "reference trajectory"

$$v = \dot{Q}_d - \Lambda e_q, \tag{14}$$

$$\dot{H} = s^T(\tau_i - M\dot{v} - Cv - g). \tag{15}$$

and choose the following control law [11]

$$\tau_i = M(Q)\dot{v} + C(Q,\dot{Q})v + g(Q) + u. \tag{16}$$

Then, substituting (16) into (2) and (15) yields

$$M(Q)\dot{s} + C(Q,\dot{Q})s = u, \tag{17}$$

$$\dot{H} = s^T u, \tag{18}$$

Equation (17) means the passivity of the closed-loop manipulator dynamics (2) from the input torque u to the output s with respect to the storage function defined in eq. (6). We can set the new control law [11]

$$u = -K_v s = -K_v\left(\dot{e}_Q + \Lambda e_Q\right), \tag{19}$$

with K_v a diagonal positive gain matrix. The final control law is given as

$$\tau_i = M(Q)\dot{v} + C(Q,\dot{Q})v + g(Q) - K_v s. \tag{20}$$

4. SLIDING MODE OBSERVER DESIGN

The control law of eq. (20) requires the measurement of joint angles, flexible modes, and their respective derivatives. To reduce the number of sensors, we develop a sliding mode observer to estimate both rigid and flexible states. The state space representation of the nonlinear system defined in (2) can be written as follows:

$$\begin{cases} \dot{x} = f(x,\tau_i), \\ y = h(x) = x, \end{cases} \tag{21}$$

where $f(x,\tau_i) = M(Q)^{-1}\left(\tau_i - C\left(Q,\dot{Q}\right)\dot{Q} + g(Q)\right)$ y is the controlled output. We assume that f, h are continuous, bounded, and differentiable nonlinear functions. To get the triangular form of the dynamical model, we define the state vector x as

$$\mathbf{x} = \left[x_1, x_2, x_3, x_4, x_5, x_6, x_7, x_8, x_9, x_{10}, x_{11}, x_{12}\right]^{\mathrm{T}}$$
$$= \left[\theta_1, \dot{\theta}_1, \theta_2, \dot{\theta_2}, q_{11}, \dot{q_{11}}, q_{12}, \dot{q}_{12}, q_{21}, \dot{q}_{21}, q_{22}, \dot{q}_{22}\right]^{\mathrm{T}}.$$

From (3), the triangular representation of the nonlinear system defined in (2) can be written as follows:

$$\begin{aligned}
\dot{x_1} &= x_2 \\
\dot{x_2} &= f_1(x,\tau_1) = \frac{\tau_1 - M_{12}\ddot{\theta}_2 - M_{13}\ddot{q}_{11} - M_{14}\ddot{q}_{12} - M_{15}\ddot{q}_{21} - M_{16}\ddot{q}_{22} - C_1(Q,\dot{Q})\dot{Q} - g_1(Q)}{M_{11}} + \delta_1(x), \\
\dot{x_3} &= x_4, \\
\dot{x_4} &= f_2(x,\tau_2) = \frac{\tau_2 - M_{23}\ddot{q}_{11} - M_{24}\ddot{q}_{12} - M_{25}\ddot{q}_{21} - M_{26}\ddot{q}_{22} - C_2(Q,\dot{Q})\dot{Q} - g_2(Q)}{M_{22}} + \delta_2(x), \\
\dot{x_5} &= x_6, \\
\dot{x_6} &= f_3(x) = \frac{-M_{34}\ddot{q}_{12} - M_{35}\ddot{q}_{21} - M_{36}\ddot{q}_{22} - C_3(Q,\dot{Q})\dot{Q} - g_3(Q)}{M_{33}} + \delta_3(x), \\
\dot{x_7} &= x_8, \\
\dot{x_8} &= f_4(x) = \frac{-M_{45}\ddot{q}_{21} - M_{46}\ddot{q}_{22} - C_4(Q,\dot{Q})\dot{Q} - g_4(Q)}{M_{44}} + \delta_4(x), \\
\dot{x_9} &= x_{10}, \\
\dot{x_{10}} &= f_5(x) = \frac{-M_{56}\ddot{q}_{22} - C_5(Q,\dot{Q})\dot{Q} - g_5(Q)}{M_{55}} + \delta_5(x), \\
\dot{x_{11}} &= x_{12}, \\
\dot{x_{12}} &= f_6(x) = \frac{-C_6(Q,\dot{Q})\dot{Q} - g_6(Q)}{M_{66}} + \delta_6(x).
\end{aligned} \tag{22}$$

Assumption 1:

The system (22) is observable, bounded input, bounded output, and stable for a finite time $t \in [0, T]$.

Assumption 2:

$\delta_1(x), \delta_2(x) .., \delta_6(x)$ present the uncertainties and disturbances. They are bounded by: $\delta_1(x) < \rho_1$, $\delta_2(x) < \rho_2$,..,$\delta_6(x) < \rho_6$, where $\rho_1, \dots \rho_6$ are known positive constants. The sliding mode observer has the following dynamics [12]

$$\begin{cases} \dot{\hat{x}} = f(\hat{x},\tau_i) + L\,\mathrm{sign}(y-\hat{y}), \\ \hat{y} = h(\hat{x}) = \hat{x}, \end{cases} \tag{23}$$

it's a copy of the state space model plus a correction term $L\,\mathrm{sign}(y-\hat{y})$, which establishes the convergence of the estimated state $\hat{x}$ to its real state x in finite time.

We note that "sign" is the classical function and L is a diagonal positive gain matrix whose diagonal elements are L_j $(j = 1,2 \dots, 12)$.

Equation (23) can be written in the triangular form as:

$$\begin{cases}
\dot{\widehat{x_1}} = \widehat{x_2} + L_1\mathrm{sign}(x_1 - \widehat{x_1}) \\
\dot{\widehat{x_2}} = f_1(\hat{x},\tau_1) + L_2\mathrm{sign}(x_2 - \widehat{x_2}) \\
\dot{\widehat{x_3}} = \widehat{x_4} + L_3\mathrm{sign}(x_3 - \widehat{x_3}) \\
\dot{\widehat{x_4}} = f_2(\hat{x},\tau_2) + L_4\mathrm{sign}(x_4 - \widehat{x_4}) \\
\dot{\widehat{x_5}} = \widehat{x_6} + L_5\mathrm{sign}(x_5 - \widehat{x_5}) \\
\dot{\widehat{x_6}} = f_3(\hat{x}) + L_6\mathrm{sign}(x_6 - \widehat{x_6}) \\
\dot{\widehat{x_7}} = \widehat{x_8} + L_7\mathrm{sign}(x_7 - \widehat{x_7}) \\
\dot{\widehat{x_8}} = f_4(\hat{x}) + L_8\mathrm{sign}(x_8 - \widehat{x_8}) \\
\dot{\widehat{x_9}} = \widehat{x_{10}} + L_9\mathrm{sign}(x_9 - \widehat{x_9}) \\
\dot{\widehat{x_{10}}} = f_5(\hat{x}) + L_{10}\mathrm{sign}(x_{10} - \widehat{x_{10}}) \\
\dot{\widehat{x_{11}}} = \widehat{x_{12}} + L_{11}\mathrm{sign}(x_{11} - \widehat{x_{11}}) \\
\dot{\widehat{x_{12}}} = f_6(\hat{x}) + L_{12}\mathrm{sign}(x_{12} - \widehat{x_{12}})
\end{cases} \tag{24}$$

By choosing appropriate parameters L_j for any initial conditions, the estimated state variables converge to the real system state variables in finite time.

The observation error e_{obs} is given as

$$e_{obs} = y - \hat{y} = x - \hat{x}, \tag{25}$$

Proof: The dynamics of the observer errors are expressed as

$$\dot{e}_{obs} = \dot{x} - \dot{\hat{x}}, \tag{26}$$

$$\begin{pmatrix} \dot{e_1} \\ \dot{e_2} \\ \dot{e_3} \\ \dot{e_4} \\ \dot{e_5} \\ \dot{e_6} \\ \dot{e_7} \\ \dot{e_8} \\ \dot{e_9} \\ \dot{e}_{10} \\ \dot{e}_{11} \\ \dot{e}_{12} \end{pmatrix} = \begin{pmatrix}
x_2 - \widehat{x_2} - L_1 sign(x_1 - \widehat{x_1}) \\
f_1(x,\tau_1) - f_1(\hat{x},\tau_1) - L_2 sign(x_2 - \widehat{x_2}) + \delta_1(x) \\
x_4 - \widehat{x_4} - L_3 sign(x_3 - \widehat{x_3}) \\
f_2(x,\tau_1) - f_2(\hat{x},\tau_1) - L_4 sign(x_4 - \widehat{x_4}) + \delta_2(x) \\
x_6 - \widehat{x_6} - L_5 sign(x_5 - \widehat{x_5}) \\
f_3(x) - f_3(\hat{x}) - L_6 sign(x_6 - \widehat{x_6}) + \delta_3(x) \\
x_8 - \widehat{x_8} - L_7 sign(x_7 - \widehat{x_7}) \\
f_4(x) - f_4(\hat{x}) - L_8 sign(x_8 - \widehat{x_8}) + \delta_4(x) \\
x_{10} - \widehat{x_{10}} - L_9 sign(x_9 - \widehat{x_9}) \\
f_5(x) - f_5(\hat{x}) - L_{10} sign(x_{10} - \widehat{x_{10}}) + \delta_5(x) \\
x_{12} - \widehat{x_{12}} - L_{11} sign(x_{11} - \widehat{x_{11}}) \\
f_6(x) - f_6(\hat{x}) - L_{12} sign(x_{12} - \widehat{x_{12}}) + \delta_6(x)
\end{pmatrix} = \begin{pmatrix}
e_2 - L_1 sign(e_1) \\
f_1(x,\tau_1) - f_1(\hat{x},\tau_1) - L_2 sign(e_2) + \delta_1(x) \\
e_4 - L_3 sign(e_3) \\
f_2(x,\tau_1) - f_2(\hat{x},\tau_1) - L_4 \mathrm{sign}(e_4) + \delta_2(x) \\
e_6 - L_5 \mathrm{sign}(e_5) \\
f_3(x) - f_3(\hat{x}) - L_6 \mathrm{sign}(e_6) + \delta_3(x) \\
e_8 - L_7 \mathrm{sign}(e_7) \\
f_4(x) - f_4(\hat{x}) - L_8 \mathrm{sign}(e_8) + \delta_4(x) \\
e_{10} - L_9 \mathrm{sign}(e_9) \\
f_5(x) - f_5(\hat{x}) - L_{10} sign(e_{10}) + \delta_5(x) \\
e_{12} - L_{11} sign(e_{11}) \\
f_6(x) - f_6(\hat{x}) - L_{12} sign(e_{12}) + \delta_6(x)
\end{pmatrix}. \tag{27}$$

We define the sliding surfaces vector as

$$\mathrm{S} = \begin{pmatrix} s_1 \\ s_2 \\ s_3 \\ s_4 \\ s_5 \\ s_6 \end{pmatrix} = \begin{pmatrix} e_2 \\ e_4 \\ e_6 \\ e_8 \\ e_{10} \\ e_{12} \end{pmatrix} = \begin{pmatrix} \dot{e_1} + L_1 sign(e_1) \\ \dot{e_3} + L_3 sign(e_3) \\ \dot{e_5} + L_5 sign(e_5) \\ \dot{e_7} + L_7 sign(e_7) \\ \dot{e_9} + L_9 sign(e_9) \\ \dot{e_{11}} + L_{11} sign(e_{11}) \end{pmatrix} \tag{28}$$

Step 1:

While the input τ_i is bounded, the state x does not go to infinity in finite time. Therefore, if $\hat{x}_1$ it is bounded, all the states of the observer are also bounded during step 1. Consequently, the observation error state is also bounded. Now, setting the following Lyapunov functions:

$$V_1 = \frac{1}{2}{e_1}^2, V_3 = \frac{1}{2}{e_3}^2, V_5 = \frac{1}{2}{e_5}^2, V_7 = \frac{1}{2}{e_7}^2, V_9 = \frac{1}{2}{e_9}^2,$$
$$V_{11} = \frac{1}{2}{e_{11}}^2. \quad (29)$$

Then their time derivatives are

$$\begin{aligned}
\dot{V}_1 &= e_1\dot{e}_1 = e_1(e_2 - L_1 sign(e_1))\\
\dot{V}_3 &= e_3\dot{e}_3 = e_3(e_4 - L_3 sign(e_3))\\
\dot{V}_5 &= e_5\dot{e}_5 = e_5(e_6 - L_5 sign(e_5))\\
\dot{V}_7 &= e_7\dot{e}_7 = e_7(e_8 - L_7 sign(e_7))\\
\dot{V}_9 &= e_9\dot{e}_9 = e_9(e_{10} - L_9 sign(e_9))\\
\dot{V}_{11} &= e_{11}\dot{e}_{11} = e_{11}(e_{12} - L_{11} sign(e_{11})) \quad (30)
\end{aligned}$$

By choosing

$$\begin{aligned}
L_1 &> \max|e_2|,\\
L_3 &> \max|e_4|,\\
L_5 &> \max|e_6|,\\
L_7 &> \max|e_8|,\\
L_9 &> \max|e_{10}|,\\
L_{11} &> \max|e_{12}|, \quad (31)
\end{aligned}$$

for a finite time, $t<T$, the observation errors e_1, $e_3, e_5, e_7, e_9, e_{11}$ tend toward zero in finite time, and consequently, $\dot{e}_1 = \dot{e}_3 = \dot{e}_5 = \dot{e}_7 = \dot{e}_9 = \dot{e}_{11} = 0$, which implies that

$$\begin{aligned}
e_2 &= L_1\text{sign}(e_1),\\
e_4 &= L_3\text{sign}(e_3),\\
e_6 &= L_5\text{sign}(e_5),\\
e_8 &= L_7\text{sign}(e_7),\\
e_{10} &= L_9\text{sign}(e_9),\\
e_{12} &= L_{11}\text{sign}(e_{11}). \quad (32)
\end{aligned}$$

Step 2:

We have

$$\dot{e}_1 = \dot{e}_3 = \dot{e}_5 = \dot{e}_7 = \dot{e}_9 = \dot{e}_{11} = 0, \quad (33)$$

and

$$\begin{aligned}
\dot{e}_2 &= -L_2\text{sign}(e_2) + \delta_1(x),\\
\dot{e}_4 &= -L_4\text{sign}(e_4) + \delta_2(x),\\
\dot{e}_6 &= -L_6\text{sign}(e_6) + \delta_3(x),\\
\dot{e}_8 &= -L_8\text{sign}(e_8) + \delta_4(x),\\
\dot{e}_{10} &= -L_{10}\text{sign}(e_{10}) + \delta_5(x),\\
\dot{e}_{12} &= -L_{12} sign(e_{12}) + \delta_6(x). \quad (34)
\end{aligned}$$

The new Lyapunov functions are

$$\begin{aligned}
V_2 &= \tfrac{1}{2}(e_1^2 + e_2^2),\\
V_4 &= \tfrac{1}{2}(e_3^2 + e_4^2),\\
V_6 &= \tfrac{1}{2}(e_5^2 + e_6^2),\\
V_8 &= \tfrac{1}{2}(e_7^2 + e_8^2),\\
V_{10} &= \tfrac{1}{2}(e_9^2 + e_{10}^2),\\
V_{12} &= \tfrac{1}{2}(e_{11}^2 + e_{12}^2), \quad (35)
\end{aligned}$$

Referring to eq. (30), the respective time derivatives of the Lyapunov functions are expressed as

$$\begin{aligned}
\dot{V}_2 &= e_2\,\dot{e}_2 = e_2\big(-L_2\text{sign}(e_2) + \delta_1(x)\big),\\
\dot{V}_4 &= e_4\dot{e}_4 = e_4(-L_4\text{sign}(e_4) + \delta_2(x)),\\
\dot{V}_6 &= e_6\dot{e}_6 = e_6(-L_6\text{sign}(e_6) + \delta_3(x)),\\
\dot{V}_8 &= e_8\dot{e}_8 = e_8(-L_8\text{sign}(e_8) + \delta_4(x)),\\
\dot{V}_{10} &= e_{10}\dot{e}_{10} = e_{10}\big(-L_{10}\text{sign}(e_{10}) + \delta_5(x)\big),\\
\dot{V}_{12} &= e_{12}\dot{e}_{12} = e_{12}\big(-L_{12}\text{sign}(e_{12}) + \delta_6(x)\big). \quad (36)
\end{aligned}$$

To ensure the negativeness of $\dot{V}_2, \dot{V}_4, \dot{V}_6, \ldots, \dot{V}_{12}$, we must choose $L_2 > \rho_1$, $L_4 > \rho_2$, $L_6 > \rho_3$, $L_8 > \rho_4$, $L_{10} > \rho_5$, $L_{12} > \rho_6$. The overall schematics of the proposed approach (Controller +observer) are depicted below (Fig. 2)

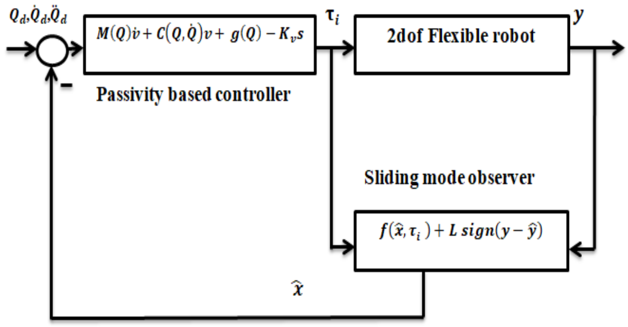

Fig.2 –Sliding mode observer schematics.

5. SIMULATION RESULTS

In this section, simulation results are presented using a fourth-order Runge-Kutta method in the MATLAB/Simulink environment to demonstrate trajectory tracking with the suggested controller. The reference trajectory is expressed as

$$\begin{cases} \theta_1 = 2\sin(0.1\pi t) \\ \theta_2 = 2\sin(0.2\pi t) \end{cases} \quad (37)$$

The system's physical parameters are listed in Table 1 [13].

Table 1

Physical parameters of the flexible arm.

Parameter	Symbol	Nominal value
Hub inertia	*Jh*1= *Jh*2	1 Kg m^2
Beam length	*L*1=*L*2	0.5m
Beam linear density	$\boldsymbol{\rho}$1= $\boldsymbol{\rho}$2	1 Kg/m
Beam rigidity	*EI*1=*EI*2	10N m^2
Payload mass	*Mp*	0.1 Kg
Hub mass	*mh*1=*mh*2	1 Kg
Payload inertia	*Jp*	0.0005Kg.m^2
Moment of inertia	*J*01= *J*02	0.0415 Kg.m^2

Figures 3 and 4 depict the PBC controller's precise tracking with minimal error and low overshoot despite the inherent structural flexibility of the arm. This confirms that while flexibility introduces visible oscillations at the tip, the control system effectively manages their magnitude, ensuring the endpoint accurately reaches its target position with acceptable residual vibration.

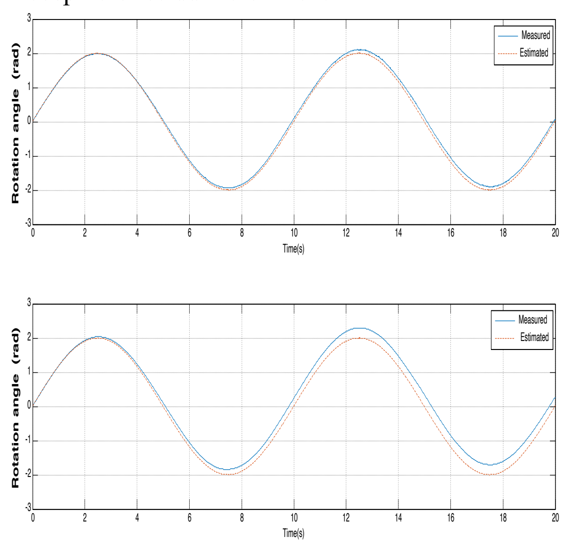

Fig. 3 – Trajectory tracking for the two links.

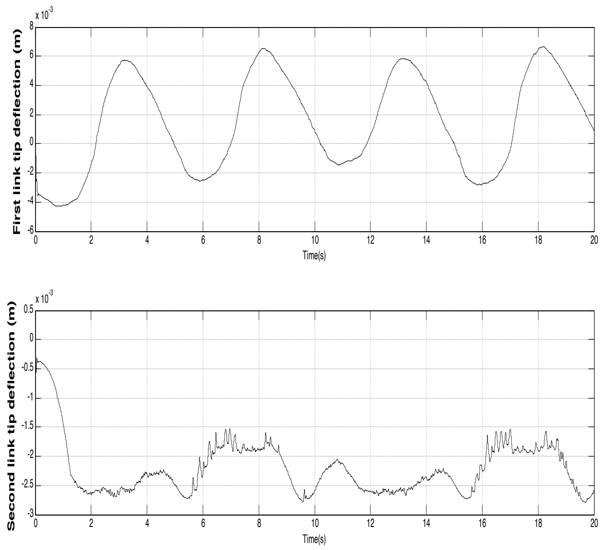

Fig. 4 – Tips deflections.

The figures (5-6) compare the performance of the sliding mode observer with that of the basic PBC controller (without an observer). It compares the measured and estimated state variables provided by the observer $[\dot{\theta}_1, \dot{\theta}_2, \dot{q}_{11}, \dot{q}_{12}, \dot{q}_{21}, \dot{q}_{22}]^T$.

The close alignment between the measured and estimated trajectories across all states demonstrates the observer's accuracy, which indicates the observer's ability to reconstruct unmeasured or noisy states in real time. Effective estimation of these states—especially the fast, lightly-damped flexible modes—is crucial for implementing high-performance model-based control strategies that actively damp vibrations.

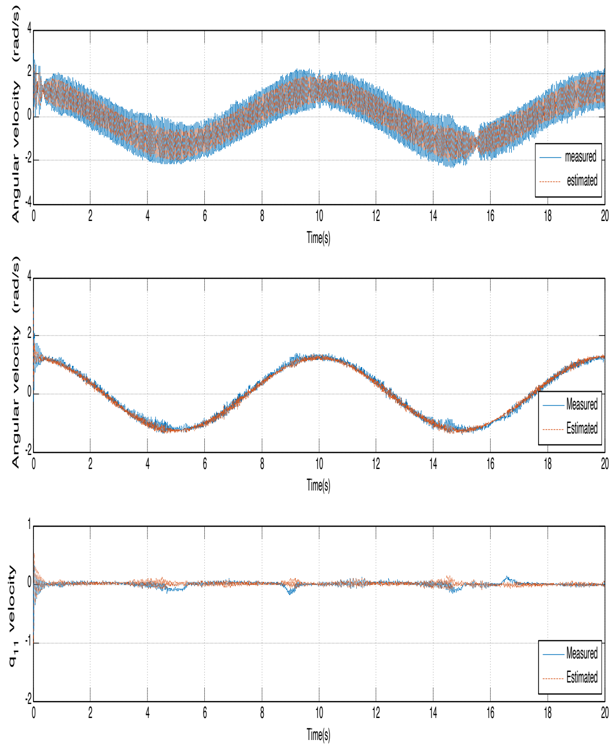

Fig. 5 – State observation performance: measured (without observer) vs. estimated values (with observer).

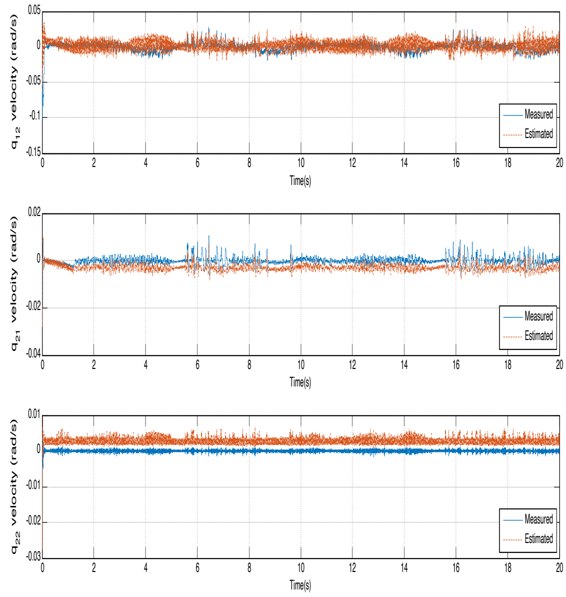

Fig. 6– State observation performance: measured vs. estimated values.

Figure 7 demonstrates the accuracy of the sliding mode observer in reconstructing the internal dynamics of the two-link flexible manipulator. The estimation error reveals consistently minimal deviations throughout the reference trajectory, bounded within 0.02 rad. Flexible mode estimation errors are also minimal, at $2x10^{-3}$ rad/s. All errors converge rapidly to near-zero following any disturbance. The design effectively rejects measurement noise, as shown by minimal high-frequency oscillations in the signals. This high-fidelity observation provides accurate full-state feedback. That feedback is a fundamental prerequisite for the passivity-based controller's success. It enables precise trajectory tracking and active damping of link vibrations.

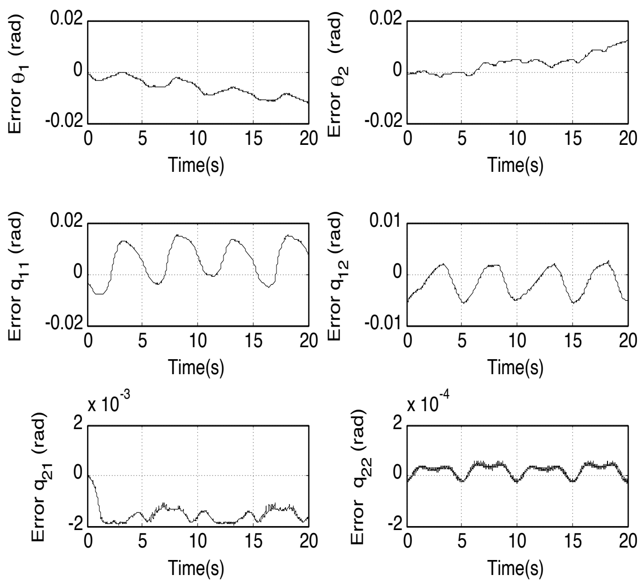

Fig. 7 – Estimation errors.

The phase portrait of a two-link flexible robot is depicted in Fig. 8; it shows a stable elliptical limit cycle, bounded within ±2 rad and ±1.2 rad/s. This closed orbit confirms periodic motion from harmonic excitation.

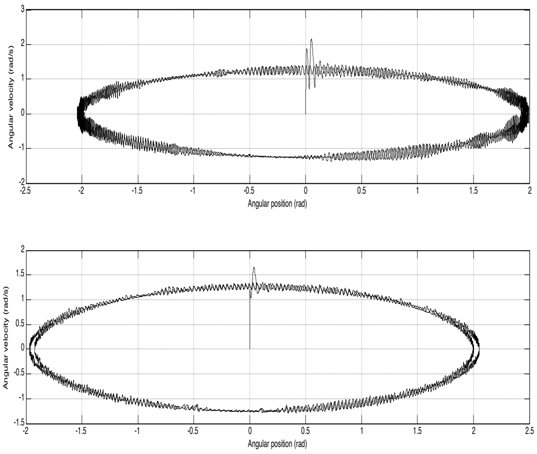

Fig. 8 – Phase portrait of a two-link flexible robot.

The ellipse arises from the interaction between link flexibility and velocity-dependent damping. Distortions along its minor axis reflect residual influences from the bending mode. Periodicity is validated by single-point Poincaré map intersections, proving effective vibration suppression. This equilibrium occurs near the natural frequency, balancing energy storage and dissipation for precise repetition.

6. **CONCLUSION**

This paper successfully developed and validated a robust control strategy for a flexible two-link robotic arm. By integrating a full-order sliding mode state observer with a passivity-based controller, the sliding mode observer offers a powerful estimation strategy, owing to its defining advantages: exceptional robustness to model uncertainties and external disturbances, and finite-time convergence of the estimation error. The Lyapunov-based stability analysis formally guarantees global system stability by leveraging the system's passivity properties. Simulation results confirm that the controller achieves accurate trajectory tracking and effectively suppresses elastic vibrations, demonstrating significant robustness against both estimation uncertainties and external perturbations

CREDIT AUTHORSHIP CONTRIBUTION STATEMENT

ADEL BELHERAZEM: conceptualization, data curation, methodology, formal analysis, investigation, resources, supervision, validation, writing – review & editing.

MOHAMED DELLA KRACHAI: formal analysis, investigation, data curation, visualization.

Zakaria BELLAHCENE: Article revision.

Received in December 2025

REFERENCES

1. A. Belherazem, R. Salim, A. Laidani, M. Chenafa, "Vibration control of a two-link flexible manipulator." Automatic Control and Computer Sciences, **58**, pp. 346–358 (2024).
2. Q. Meng, X. Lai, Z. Yan, C.Y. Su, M. Wu, "Motion planning and adaptive neural tracking control of an uncertain two-link rigid–flexible manipulator with vibration amplitude constraint." IEEE Trans. Neural Netw. Learn. Syst. (2022).
3. B. Xu, P. Zhang, "Composite learning sliding mode control of flexible-link manipulator." Complexity, article ID 9430259 (2017).
4. M. Boussoffara, I.B. Ahmed, Z. Hajaiej, "Sliding mode controller design: Stability analysis and tracking control for flexible joint manipulator." Rev. Roum. Sci. Techn. – Électrotechn. Et Énerg., **66**, *3*, pp. 161–167 (2021).
5. A. Belherazem, M. Chenafa, "Passivity-based adaptive control of a single-link flexible manipulator." Automatic Control and Computer Sciences, **55**, pp. 1–14 (2021).
6. H.M. Yatim, I.Z. Darus, M.H. Ab. Talib, M.H. Abu Bakar, "Active vibration control of flexible manipulator using genetic algorithm with parameter exchanger." IEEE 8th International Conference on Smart Instrumentation, Measurement and Applications (ICSIMA) (2022).
7. H. Djerbi, I. Al-Darraji, G. Tsaramirsis, M. Khchaou, R. Abbassi, O. Alshammari, "Fuzzy Luenberger observer design for nonlinear flexible joint robot manipulator." Electronics, 11, 10 (2022).
8. D.H. Bui.Phuc, J.A. Scultz, "A semilinear parameter-varying observer method for fabric-reinforced soft robots." Frontiers in Robotics and AI, **8** (2021).
9. M. Khairudin, Z. Mohamed, A.R. Husain, M.A. Ahmad, "Dynamic modeling and characterization of a two-link flexible robot manipulator." Journal of Low Frequency Noise, Vibration and Active Control, pp. 207–219 (2010).
10. M.W. Spong, M. Vidyasagar, S. Hutchinson, "Robot modelling and control." John Wiley & Sons (2006).
11. T. Hatanaka, N. Chopra, M. Fujita, M. Spong, "Passivity-based control and estimation in networked robotics." Communication and Control Engineering, Springer (2015).
12. J.P. Barbot, T. Boukhobza, M. Djemai, "Sliding mode observer for triangular input form." Proceedings of the 35th IEEE Conference on Decision and Control (1996).
13. A. Belherazem. *Commande Non Linéaire Robuste D'un Bras Manipulateur Flexible,* Thèse de doctorat, ENP Oran (2022).
14. L. Li, F. Cao, J. Liu, "Vibration control of flexible manipulator with unknown control direction." International Journal of Control, **94**, *10*, pp. 2690–2702 (2021).
15. A. Belherazem, Z. Bellahcene, A. Laidani, "Passivity-based control of a two-link flexible manipulator." The 1st International Conference on Advances in Electronics, Control and Computer Technologies ICAECT'23, Mascara, Algeria (2023).
16. W. Nan, H. Qin, "A velocity self-learning algorithm for time-optimal trajectory planning along the fully specified path - Part I." Rev. Roum. Sci. Techn. – Électrotechn. Et Énerg., **70**, 1, pp. 109–114 (2025).
17. W. Nan, H. Qin, "A velocity self-learning algorithm for time-optimal trajectory planning along the fully specified path - Part II." Rev. Roum. Sci. Techn. – Électrotechn. Et Énerg., **70**, 1, pp. 241–246 (2025).